Photolysis at the Speed of Light: Chemical Free Degradation of Trace Organic Contaminants by Bespoke Photolysis Using High Intensity UV LEDs

Jessica L. Bennett[a], Sean A. MacIsaac[a], Jin Li[a], Metyn B. Rehman[a], Rae E. Fitzgerald[a], Amina K. Stoddart[a], and Graham A. Gagnon[a*]

[a]Centre for Water Resources Studies, Faculty of Engineering, Dalhousie University, Halifax, NS, Canada

[*] Corresponding Author:

Email: Graham.Gagnon@dal.ca

Address: Department of Civil and Resource Engineering, Dalhousie University, 1360 Barrington St. Halifax, NS, Canada (B3H 4R2)

Phone: 902-494-3972

Abstract

UV LEDs have demonstrated effectiveness in disinfection applications and proven suitability at scale for disinfection in municipal wastewater and drinking water. Technological advances in materials design and electrical efficiency have made high-intensity light delivery by UV C LEDs a reality and now poise these traditionally disinfection system to serve a dual purpose for targeted remediation of trace contaminants. This work investigated the effectiveness of UV C light emission tailoring on the photodegradation dynamics of select trace organic compounds (TrOCs). Degradation kinetics and quantum yields of target compounds under 275 nm irradiation were governed by molar absorbance and chemical structure, and kinetics followed estrone (E1) > tryptophan > caffeine ≈ pCBA > urea. Secondary experiments compared the efficacy of a 275 nm UV LED and medium-pressure mercury vapour (MP UV) system for photodegradation of two steroid estrogens, E1 & 17β-estradiol (17β-E2). Use of the 275 nm UV LED system substantially reduced fluence requirements to achieve 90% degradation of both compounds. LC-MS/MS analysis of E1 photodegradation products showed that the UV LED system was more effective in eliminating both the E1 and its associated photoproduct compared to the MP UV system. This work demonstrates the effective use of UV LEDs for tailored photolysis of TrOCs and provides evidence for their use potential in applications outside of water disinfection.

Graphical Abstract

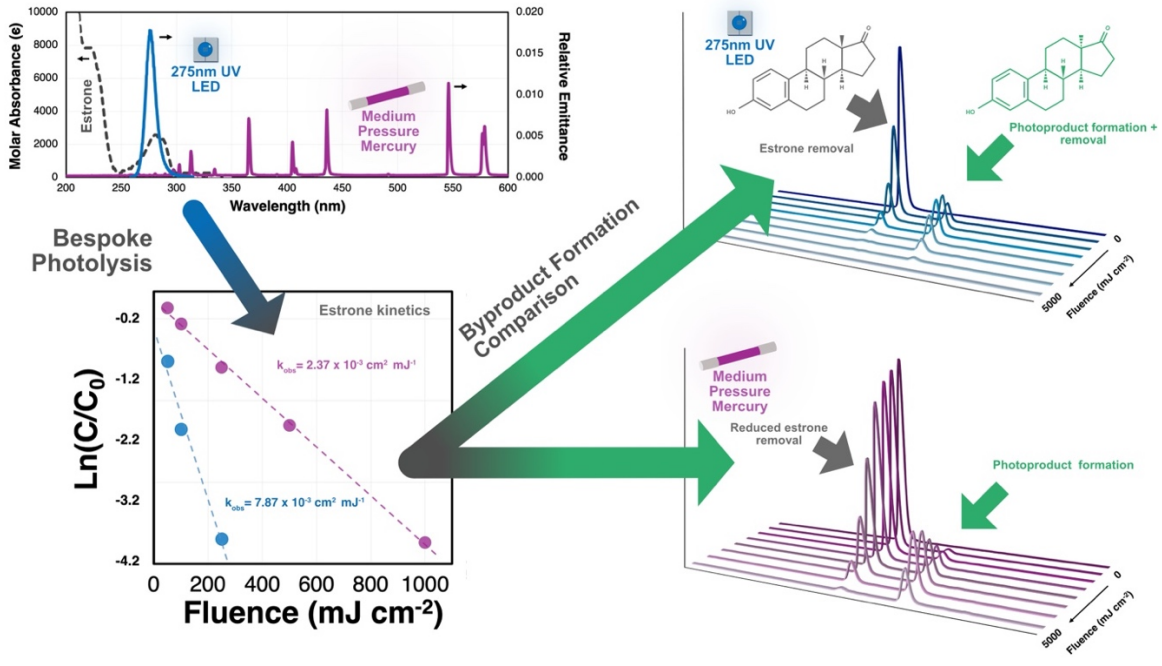

1 INTRODUCTION

The widespread use of UV light in water treatment has long been recognized as a safe and effective method to inactivate pathogenic organisms and ensure water safety. UV water treatment systems were first produced commercially in the 1930's and are now commonplace in municipal and industrial applications. Commercial UV treatment systems currently rely on the use of mercury-based UV light-emitting lamps which have historically been the only industry-ready UV treatment devices commercially available. The use of mercury in commercial and consumer products is being sequentially phased out in the European Union via *Regulation - 2024/1849*[1]. The United Nations Minamata Convention, currently supported by 128 signatories, is set to ban mercury mining by 2032[2]. Mercury has long been known for its neurotoxicity effects[3], and the realities of mercury mining can result in long-lasting environmental and human-health effects to both miners and those living in affected regions[4,5]. It is therefore not only necessary to evaluate and validate technological water treatment alternatives to comply with current and future regulations, but also to ensure safe development and sourcing of materials used in consumer and industrial products.

The emergence of solid-state light emitters (SSLEs), such as light-emitting diodes (LEDs), revolutionized consumer technology industries in the mid-20th century[6,7]. Today, SSLE devices can be found in almost all consumer and industrial devices requiring illumination. The versatility, adaptability, and efficiency of SSLEs has opened the door to illumination technologies that would not be possible with historical lighting alternatives. While visible and infrared light LEDs have been commercially available since the 1970s, UV-emitting solid-state light sources, or UV LEDs, have only become available to consumer and industrial markets in the last two decades[6] and are now poised to disrupt the water treatment industry analogously to SSLEs in technological applications.

UV LEDs have many inherent properties that provide benefits over commercially available mercury-vapour systems[6,8,9]. UV LED devices are made of semiconductor chips which can be densely packed into UV reactors to provide effective and uniform treatment. Their design

versatility and ability to run on battery power also makes them an adaptable measure for point-of-use applications such as at-the-tap water disinfection for isolated areas (e.g., campgrounds, portable water disinfection devices). The dimmable nature of UV LEDs allows ramping up or down of UV intensity in cases where water quality is affected by seasonal dynamics, whereas mercury lamps are designed to operate at a stable, consistent brightness as frequent lamp cycling truncates the lifecycle of conventional systems. UV LEDs have proven effective for disinfection in small-scale[10] and decentralized drinking water systems[11], biofilm-based *Pseudomonas aeruginosa*[12], and most recently for a full-scale 2-MLD wastewater treatment system[13].

UV LEDs wavelength emission can be tailored dependant on treatment application. Unlike commercially available mercury-vapour lamps which emit monochromatically at 253.7 or 365 nm, or polychromatically between 200 – 600 nm, UV LEDs emit light within narrow wavelength bands (i.e., full-width at half-maximum (FWHM) ~ 10-15 nm) which are dependent on the band gap energy of the employed semiconductor materials[8]. Most current generation UV LEDs are composed of $Al_xGa_{1-x}N$ semiconductor materials, which are non-toxic, UV transparent and materially conductive[6]. The composition of the $Al_xGa_{1-x}N$ material can be theoretically adjusted to achieve wavelength emission regions ranging from 210 – 365 nm[14]. The versatility in emittance wavelength of $Al_xGa_{1-x}N$-based UV LEDs makes them adaptable to treatment applications requiring light in wide ranges of the electromagnetic spectrum (i.e., UV A – UV C)[6]. The potential for bespoke UV LED treatment through specific wavelengths has demonstrated flexibility to target specific biomarkers and thereby lower required UV fluence to achieve pathogen inactivation objectives[15–18].

Photolytic degradation of chemical contaminants can be optimized by tailoring UV LED wavelength emission to the absorbance spectrum of a compound of interest. Photons emitted within the typical UV treatment region of the electromagnetic spectrum (i.e., 300 nm – 200 nm) have energies ranging from 4.13 – 6.2 eV or 95.2 – 143 kcal mol^{-1} which is sufficient to break most chemical bonds (e.g., C-H bonds in alkanes have bond dissociation energies (BDEs) ranging

from 94 – 99 kcal mol^{-1} while BDEs in C-C bonds range from 77 – 83 kcal mol^{-1} in aliphatic compounds[19]). Wavelength-specific photolysis of chemical contaminants has been limitedly investigated[9,19–23], but technological advancements and significant improvements in power output have made delivery of high-intensity UV light from LED sources a reality[8]. This advancement along with wavelength tuneability and development of high-density reactors poise UV LEDs to be a disruptive technology for which beyond disinfection is possible.

Here, we evaluate the efficacy of UV C LEDs to degrade trace organic compounds (TrOCs) through photolysis-initiated reactions and introduce a novel, high-intensity flow-through UV C LED reactor which provides high fluence delivery (i.e., > 1000 mJ cm^{-2}) in a matter of seconds. We also evaluate the impact of compound-specific parameters to infer both practical and theoretical potential for UV C LED photolytic degradation and compare UV C LED treatment effectiveness and electrical efficiency to traditional MP UV systems under collimated beam setups. Finally, we discuss future potential and application for UV C LEDs as a chemical-free water treatment tool and replacement for mercury-vapour lamps. TrOCs are notoriously difficult to remove and abate using traditional water treatment technologies and can cause unintended issues when interacting with conventional chemical disinfectants. Wavelength dependant interactions between TrOCs and light are not well understood across the UV C spectrum but there are indications that photolysis alone could help mitigate unintended byproduct formation[24]. The use of tailored UV reactors will lead to a future that does not require the use of chlorine, ozone, or peroxide for the removal of emergent contaminants while also removing mercury from the treatment process.

2 MATERIALS AND METHODS

2.1 Chemicals and Reagents

ACS grade 4-Chlorinebenzoic acid (pCBA), caffeine, tryptophan, and urea, were sourced from Sigma-Aldrich. 1g/L stocks of E1 and 17β-E2 (dissolved in methanol or acetonitrile) were

obtained from Cerilliant Co. (Texas, USA). Working solutions of each of the target compounds were prepared from the neat chemical standards at a concentration of 1 g L^{-1} in water, apart from E1 & 17β-E2 which were spiked directly from their purchased 1 g L^{-1} stock in methanol and acetonitrile (respectively). LCMS-grade methanol, LCMS-grade formic acid, and Optima acetonitrile used in LC-MS/MS and HPLC-UV/Vis analysis were purchased from Fisher Scientific. Laboratory-grade water with a resistivity of 18.2 mΩ cm^{-1} and total organic carbon (TOC) < 5 µg L^{-1} was sourced from a Milli-Q purification system (Reference A+, Millipore) was used for the preparation of all chemical solutions and reagents.

2.2 Model Compound Selection

Initial photolysis experiments (Part 1) using the 275 nm UVC LED flow-through reactor were conducted using a range of organic compounds including: 4-chlorobenzoic acid (pCBA), commonly used as a probe compound for estimation of $OH^{\bullet}$ radical exposure in AOP systems[37,72]; urea, a major waste product in municipal wastewater, industrial, and agricultural effluent streams[73]; tryptophan, an amino acid indicative of microbial activity in biological systems[74,75]; caffeine, an alkaloid and a probe compound for $OH^{\bullet}$ and reactive chlorine species (RCS)[76] and a tracer for anthropogenic contamination; and two steroid estrogens, E1 & 17β-E2. These compounds were chosen to the differing structure, molar absorbance in the 275 nm emittance range and sensitivity to UV C irradiation.

Secondary experiments (Part 2) were conducted using two steroid hormones (E1 and 17β-E2) as target compounds to evaluate and compare their response to 275 nm UV C LED and MP UV irradiation in collimated beam setups. These compounds were chosen for secondary experiments as they are well known TrOCs that are of environmental concern[55] and exhibit differing sensitivity to UVC irradiation[29,32,35]. The chemical structure, CAS number, and molar mass of each of the described compound is given in Figure SI-1 while their absorbance spectra can be found in Figure 2.

2.3 Reactor Characteristics and Design

2.3.1 Flow-Through UVC LED Reactor

Initial experiments were conducted using a bench-scale DC UV C LED reactor, the PearlAqua ThinFilm 534A2 (AquiSense Technologies ©), which consists of four main components: a light source assembly, a safety shield, a flow cell, and a driver assembly. The reactor contains an array of 192 UV C LED chips which emit light at a 275 nm peak emission wavelength (See Figure 2 for emission spectrum). The reactor was equipped with a 4 cm x 15 cm x 2.5 cm quartz laminar flow cell with a volume of 4.13 cm^3. A schematic of the reactor is given in Figure SI-2. The emittance spectrum of the reactor can be seen in Figure 2 while the laminar flow cell is shown in Figure SI-3.

The driver assembly houses the power supply, which converts AC electrical input to DC electrical output for the lamp assembly and transmits data via MODBUS. An intermediate coolant loop is used to cool the driver assembly and routes coolant (tap water) from the cooling block through the lamp assembly. A laptop is connected to the driver assembly and controls the lamp output via the user interface. The interface enables control of the light source assembly, the power level and senses the temperature of the internal electrical components. Coolant water was supplied via by connecting the cooling block to a barbed faucet tap using rubber hosing. The influent sample water was controlled using a peristaltic pump which was calibrated to range of flow rates (Table SI-1).

2.3.2 Collimated Beam Reactors

Secondary experiments were carried out using an Aquisense PearlBeam unit (UV LED experiments) with an average irradiance of 3.62 mW cm^{-2} (3.5 cm from the edge of the collimator) and 275 nm peak emittance, and a Calgon Carbon collimated beam unit equipped with a 1000 kW polychromatic medium-pressure lamp with an average irradiance of approximately 2.80 mW cm^{-2} measured 3.5 cm from the edge of the collimator and 200 – 600 nm spectral emittance (see Figure 3 for emittance spectrum).

2.4 Experimental Procedures

2.4.1 UV C LED Photolysis of Target Compounds Using a 275nm High-throughput Flow-Through Reactor

The starting concentration of the selected target compounds varied due to range of analytical methods required for quantitation and solubility limitations (Table SI-3). The aqueous solution of target compound was connected via rubber tubing to a water pump and the reactor. The starting sample volume was 2 L which was spiked with a concentrated working solution of target analytes to achieve target concentrations. The samples were collected from the outlet of the reactor and circulated multiple times (Table SI-1) to achieve a range of UV fluences (as determined by uridine actinometry; see Methods below). Samples were taken during each recirculation round. Experiments were carried out in triplicate. Between each sample run, an ultrapure water rinse of more than 90 seconds (approximately 150 mL) was completed at a flow rate of 100 ml min^{-1}. Sample volume collected for analysis was 10 mL. Samples undergoing LC-MS/MS quantitation (E1, 17β-E2, caffeine, & tryptophan) were fortified with their associated internal standards prior to analysis. All data at or above calculated method detection limits (MDLs) are reported as their quantitated value. Only data at or above calculated limits of quantitation (LOQs) were used in kinetics calculations. MDLs and LOQs of target compounds are given in Table SI-3.

2.4.2 Comparison of UV C LED and Medium-Pressure UV Photolysis of Steroid Estrogens

Collimated beam experiments were carried out using 50 mL water samples spiked with 10 µg L^{-1} of E1 or 17β-E2 from a 100 mg L^{-1} solution in methanol. Samples were exposed to fluences of 25 – 10 000 mJ cm^{-2} from either UV C LED (275 nm) or medium-pressure UV light sources. Samples were adjusted to pH 7 using a combination of potassium phosphate monobasic (KH_2PO_4) and potassium phosphate dibasic (K_2HPO_4) at 2 mM concentrations.

Samples were stirred constantly during treatment and equilibrated for a period of 1 min before starting experiments. 240 µL aliquots were removed from the 50 mL sample throughout the experiment at time points corresponding to chosen UV doses. The smallest possible aliquot volume was used as to not significantly affect the pathlength of the water sample and subsequently the UV fluence received by the water matrix (< 5% change in sample volume). 240 µL aliquots were placed in 2 mL microcentrifuge tubes, fortified with 40 µg L^{-1} $^{13}C_6$-17β-E2 internal standard, and transferred to 2-mL amber autosampler vials before being analyzed via LC-MS/MS. All data at or above calculated method detection limits (MDLs) are reported. Only data at or above the calculated limits of quantitation (LOQs) were used in kinetics calculations.

2.4.3 Kinetics Rate Constant, Quantum Yield and Electrical Efficiency Order (EEO) Calculations

Fluence- or time-based first-order rate constants (k_{obs}) were determined for individual compounds by calculating the slope of the first order degradation plot.

$$\ln \frac{[C_A]}{[C_{0,A}]} = k_{obs} \quad (1)$$

Where $[C_{0,A}]$ is the initial concentration of compound *A* and $[C_A]$ is the concentration of compound *A* under a specific treatment condition. We calculated the polychromatic and monochromatic quantum yields (Φ) of each of the above test compounds as described in Equation 2 and 3 below [46]:

$$\Phi_{A,poly} = \left(\frac{10}{\ln(10)}\right) \frac{k_{obs,t}}{\mathrm{PF} \int_{l_2}^{l_1} \varepsilon_A(\lambda)\, E_p^0 \times \mathrm{RF}(\lambda)\mathrm{d}(\lambda)} \quad (2)$$

$$\Phi_{A,mono} = \left(\frac{10}{\ln(10)}\right) \frac{k_{obs,t}}{\mathrm{PF} \times \varepsilon_A(\lambda) E_p^0 \times \mathrm{RF}(\lambda)} \quad (3)$$

Where $\Phi_{A,poly}$ and $\Phi_{A,mono}$ are the polychromatic and monochromatic Φ of compound *A* respectively. Under 275 nm and MPUV irradiation, $\Phi_{A,poly}$ was calculated using the wavelength range of 258 – 315 nm, and 200 – 310 nm, respectively. $\Phi_{A,mono}$ was determined at 275 nm for the 275 nm peak emittance UV C LED reactors. $k_{obs,\ t}$ is the time-based first order reaction rate constant of compound *A* (s^{-1}), PF is the petri factor, RF is the reflectance factor, $\varepsilon_A(\lambda)$ is the molar absorption coefficient ($M^{-1}\ cm^{-1}$) and E_p^0 is the photon irradiance (einstein $s^{-1}\ m^{-2}\ nm^{-1}$).

In secondary experiments, Electrical efficiency order (EEO) was calculated to determine the amount of electrical energy required to reduce the concentration of E1 and 17β-E2 by one order of magnitude using Equation 6[77,78]:

$$EEO = \frac{1000Pt}{V \times \ln(C_0/C_t)} \quad (4)$$

$$P = \frac{IA}{10^6 \times \eta} \quad (5)$$

$$EEO = \frac{1000t}{V\lg(C_0/C_t)} \times \frac{IA}{10^6\eta} = \frac{\ln(10) \times It}{\ln(C_0/C_t)} \times \frac{1000A}{10^6\eta V} = \frac{0.64A}{10^6\eta V k_{obs}} \quad (6)$$

Where *P* is the incident power on the surface of the water (kW), *t* is time for sample irradiation, V is the volume of the sample, C_0 and C_t are sample concentrations before and after irradiation, *I* is the incident irradiance on the surface of the sample ($mW\ cm^{-2}$), *A* is the sample surface area (cm^2), and η = WPE for each light source (3.5 % for the 275 nm UV LEDs and 15 % for the MP UV lamp).

2.5 UV Fluence Calculations

2.5.1 Uridine Actinometry to Determine Fluence Delivery for the Flow-Through UVC LED Reactor

The irradiance of the 275 nm flow-through reactor was calculated using the methods outlined by Pousty et al. (2023)[79] and the following assumptions. The petri factor (PF) was assumed to be 1 since the irradiance of different parts of the cell should not differ within the ThinFilm Reactor. The molar absorption coefficients of uridine used in calculations were 10 185 M^{-1} cm^{-1} at 262 nm[80] and 8000 M^{-1} cm^{-1} at 275nm[81]. The calculated irradiance via uridine actinometry was 249 mW cm^{-2}. Table SI-1 outlines fluences for each target analyte throughout experimental runs which were similar to the modeled fluences provided by the manufacturer (within 15.3 %).

2.5.2 Collimated Beam Fluence Calculations

UV irradiance measurements were performed using an OceanOptics USB2000 spectroradiometer. The average fluence rate (E'_{ave}, reported in mW cm^{-2}) of each system was calculated by multiplying the incident fluence rate (E_0) measured at the center of the sample surface by correction factors described by Bolton and Linden (2003):[82]

$$E'_{ave} = E_0 \times \text{Petri Factor} \times \text{Reflection Factor} \times \text{Water Factor} \times \text{Divergence Factor} \quad (5)$$

Where the Petri Factor is ratio of the average irradiance over the area of the sample, the Reflection Factor accounts for the change in refractive index as the light beam enters water, the Water Factor accounts for light absorbed by the water matrix, and the Divergence Factor accounts for the divergence of the light beam as it exits the lamp. Sampling times were then determined by dividing E'_{ave} by the desired fluence. The integration ranges used to measure the intensity of each of the light sources were 200 – 310 nm (MP UV) and 255 – 315 nm (275 nm UV LED).

2.6 Analytical Methods

Caffeine, tryptophan, E1 and 17β-E2 were analyzed via LC-MS/MS using an Agilent 1260 liquid chromatography system and Agilent 6460 triple quadrupole mass spectrometer as previously described[60,83]. Caffeine and tryptophan were quantified under the same analysis method and a separate method was used for measurement of E1 & 17β-E2. Mass spectrometry acquisition of all compounds was conducted using multiple reaction monitoring (MRM) in either electrospray ionization (ESI) positive (caffeine & tryptophan) or negative (E1 & 17β-E2) mode. Data acquisition and analysis was carried out using Agilent MassHunter Software (Version Rev B.10.00). Detailed methods can be found in SI-Text 1 & 2 and analyte-specific parameters can be found in Table SI-2. pCBA & Urea were quantified using HPLC-UV/Vis spectroscopy and UV/Vis Spectroscopy, respectively, and detailed in in SI-Text 3 & 4. Method detection limits (MDLs) and limits of quantitation (LOQs) for all analytes were determined as per the US EPA *Definition and Procedure for the Determination of the Method Detection Limit, Revision* 2[84]. Target concentrations, analysis methods, MDLs, LOQs, and associated internal standards (where applicable) can be found in Table SI-3.

3 Results and Discussion

3.1 Part 1: Degradation of TrOCs in a High-Intensity Flow-Through UV C LED Reactor

3.1.1 Degradation and Kinetics

The PearlAqua ThinFilm reactor (AquiSense, Erlanger, KY, USA) is a high intensity flow-through UV C LED instrument which was used to assess the photodegradation of target compounds under high intensity UV C light (peak 275 nm emittance; Figure 2). The ThinFilm instrument is a tailored photolytic UV LED reactor whose UV emittance profile can be manufactured to the absorbance spectrum of a given target. Target compounds (pCBA, caffeine, urea, tryptophan, and estrone (E1))

were exposed to a range of delivered fluences (0-3200 mJ cm^{-2}; Table SI-1) to assess photodegradation dynamics. Figure 1 A-C illustrates the process flow of the tailored photolytic UV LED reactor where a working solution of a target organic compound is pumped through a flow cell and exposed to the UV C LED-generated light. The backside of the UV LED panel is cooled by an external heat exchanger that is attached to a standard water faucet. Figure 1 i-iii) shows the degradation kinetics of the five targets grouped by i) 275nm UV-resistant compounds; and ii) 275nm UV-susceptible compounds.

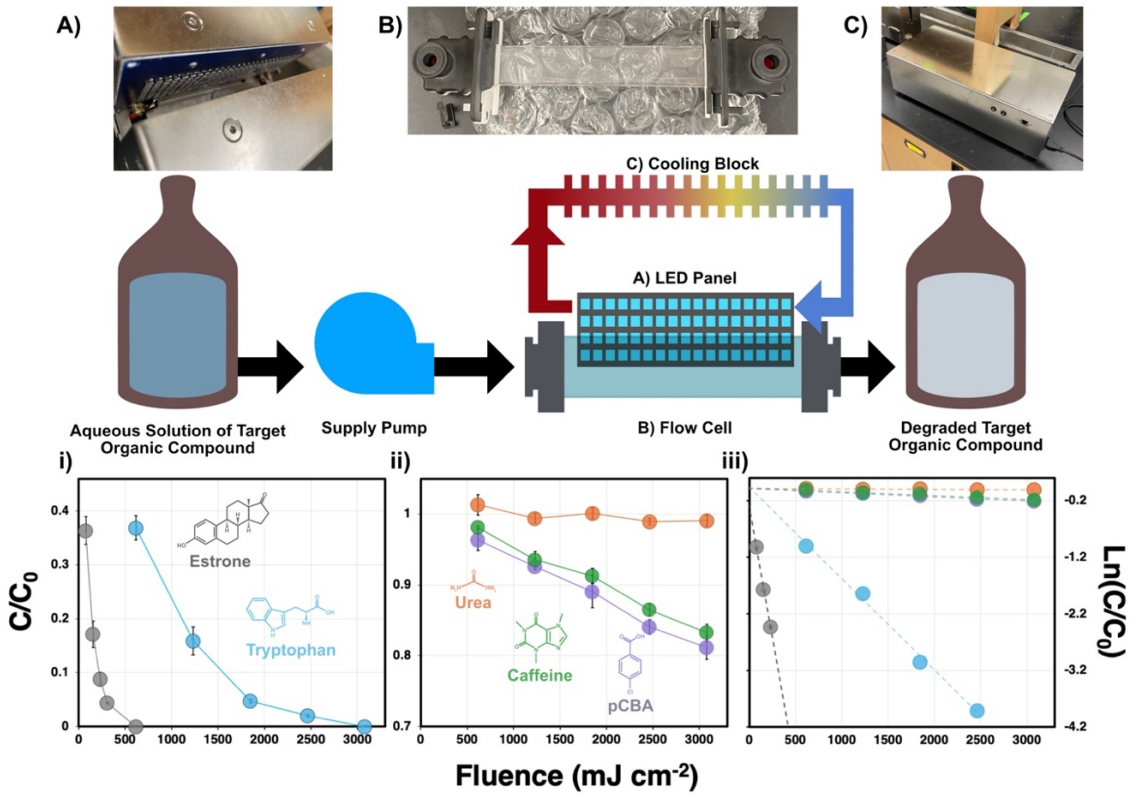

Figure 1. Degradation and first-order kinetics plots of target compounds under 275 nm irradiation from the 275 nm tailored photolytic UV LED reactor. A) LED Panel, B) Flow Cell, C) Cooling Block. i) 275 nm resistant compounds, ii) 275 nm susceptible compounds, iii) Degradation kinetics of all target compounds. pH = 7, 2 mM PO_4^{2-} buffer; $[Urea]_0$ = 50 mg L^{-1}; $[pCBA]_0$ = 10 µM; $[Caffeine]_0$ = 10 µg L^{-1}; $[Tryptophan]_0$ = 100 µg L^{-1}; $[E1]_0$ = 10 µg L^{-1}. n = 3.

The efficacy of 275 nm light in degrading each of the compounds is governed by both the spectral absorbance and the chemical structure of each compound. The photon energy absorbed by a given compound must be sufficient to overcome a given chemical bond energy for photodissociation to occur. All compounds, with the exception of urea, exhibited moderate to high molar absorbance in the emittance range of the UV LED reactor (Figure 2). The compounds that exhibited minimal degradation under 275 nm irradiation (i.e., pCBA & caffeine) followed a similar degradation profile in resisting photodissociation from 275nm light (Figure 1 i)) which is further described in later discussion.

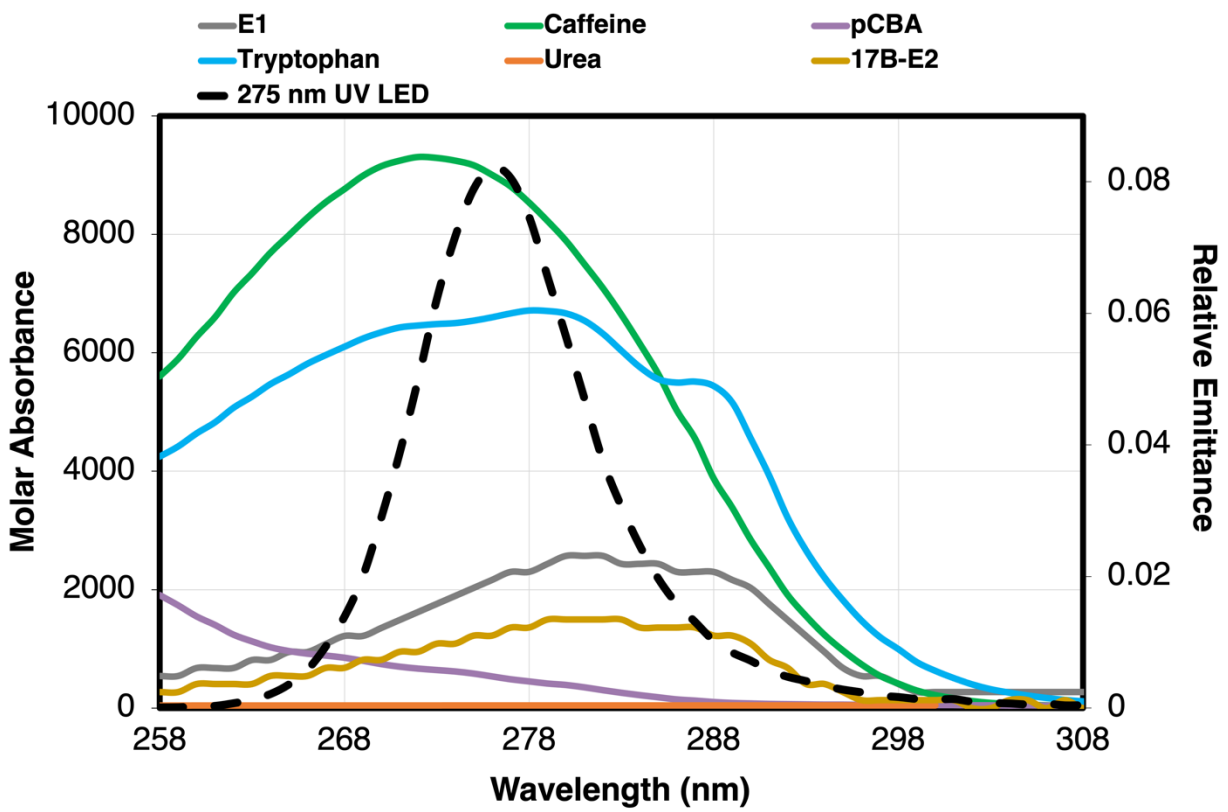

Figure 2. Molar absorbance of target compounds and relative emittance of the 275 nm UV C LED reactor.

3.1.1.1 *Degradation of Compounds Sensitive to 275 nm UV Light*

Tryptophan was degraded at the second highest rate of all target compounds evaluated and exhibited > 95% degradation (below detectible limits) at the highest fluence condition (k_{obs} = 1.62 x 10^{-3} cm^2 mJ^{-1}; Table 1). Tryptophan exhibits high absorbance in the 275 nm wavelength range (ε_{275nm} = 6543 M^{-1} cm^{-1}) which is attributed to its highly conjugated indole ring and carbonyl group on C1 (Figure SI-1). Previous work has similarly observed that tryptophan will readily degrade under UV irradiation and can both undergo direct photolysis and participate in auto-oxidation reactions to form reactive oxygen species (ROS) which can further contribute to degradation[25,26].

Table 1. Fluence-based rate constants, coefficient of determination values (r^2), and molar absorption coefficients (ε_{275nm}) for target compounds. Brackets indicate 95 % confidence intervals.

Analyte	Fluence-based rate constant k_{obs} (/x 10^{-3}; cm^2 mJ^{-1})	r^2	ε_{275nm} (M^{-1} cm^{-1})
Urea	0.00792 [0.00253, 0.0133]	0.641	0
pCBA	0.0723 [0.0601, 0.0845]	0.995	600
Caffeine	0.0661 [0.0577, 0.00745]	0.991	9884
Tryptophan	1.62 [1.57, 1.66]	0.998	6543
E1	9.22 [8.59, 9.84]	0.999	2028

E1 was degraded more rapidly than all other analytes during treatment (9.22 x 10^{-3} cm^2 mJ^{-1}; Table 1) and demonstrated > 95% removal (below detectable limits) at a fluence of 616 mJ cm^{-2} (Figure 1). The photochemistry of E1 is well documented[27–30]. E1 is known to be highly susceptible to

photolysis under LP UV, MP UV and even solar irradiation[27,31–35] and has an absorbance band around 280 nm with peak $\lambda = 281$ (Figure 2), $\varepsilon_{275nm-281nm} = 2027 - 2568\ M^{-1}\ cm^{-1}$. The presence of the phenolic ring on E1 is responsible for the observed 280 nm absorbance band while the C17 carbonyl group provides weak absorption ~290 nm[27–29] both of which overlap with the emittance of the 275 nm UV C LED reactor used in this study.

During E1 photolysis, we observed the evolution and disappearance of a photoproduct throughout treatment which had the same quantifier and qualifier ion transitions as E1 (m/z 269.1 -> 145 and 269.1 -> 143.2, respectively) with a slightly later retention time (6.62 min for E1 vs. 7.16 min for the photoproduct) as shown in Figure SI-4, SI-5 A. The ion transitions and nominal mass of the photoproduct are consistent with the 13α-epimer of E1, lumiestrone, which is structurally identical to E1 with the exception of a the rotation of the C13 methyl group and has been reported in the literature to be the primary photoproduct of E1[27,34,36]. The primary mode of E1 degradation at ~280 nm emittance is dependent on photon absorption by the phenol group and transfer of excitation to the carbonyl group, leading to epimerization and subsequent formation of lumiestrone, a reaction which is both solvent- and wavelength-dependant[27]. This energy transfer mechanism is most likely due to direct emission from the phenol group after excitation (~304 nm) which overlaps with the absorption of the carbonyl group (~290 nm)[30]. Interestingly, rapid photodegradation of E1 as compared to other steroid estrogens is well documented in the literature[27,34,35] and is most likely due to the aforementioned energy transfer mechanism as E1 is the only steroid estrogen containing a carbonyl group. We observed rapid evolution of the photoproduct with peak formation occurring at a fluence of 231 mJ cm^{-2} (Figure SI-4, SI-5 A). Photoproduct response then decreased with increasing fluence to a maximum 2464 mJ cm^{-2}, where the photoproduct was reduced by > 98% of maximum peak response observed at the 231 mJ cm^{-2} condition.

3.1.1.2 *Degradation of Compounds Resistant to 275 nm UV Light*

Urea was negligibly degraded under 275 nm irradiation and exhibited a maximum of mean < 1% removal even under the highest fluence condition (3081 mJ cm^{-2}; k_{obs} = 7.92 x 10^{-6} cm^2 mJ^{-1}; Figure 1; Table 1). Urea exhibits very low or no absorbance within the emittance range of the 275 nm LED (0–1.2 M^{-1} cm^{-1} between 258 – 315; Figure 2). Photons must be absorbed by a compound to undergo photochemical reactions (Grauss-Draper law). Degradation data for urea were a poor fit for first-order kinetics (r^2 = 0.641; Table 1) which is unsurprising due to low removal exhibited throughout experiments.

pCBA was minimally degraded during treatment and exhibited a maximum of mean 19 % removal under highest fluence conditions (k_{obs} = 7.23 x 10^{-5} cm^2 mJ^{-1}; Figure 1; Table 1). pCBA exhibits moderate absorbance within the UV C LED emittance range (Figure 2) with ε_{275nm} = 600 and thus would be capable photon absorption under this scenario. It is well known that pCBA does not readily undergo photolysis under both low-pressure (LP UV) and MP UV irradiation[37] and its photostability has made it widely used as a $OH^{\bullet}$ probe in advanced oxidative processes (AOP) studies[37–39]. The low reaction rate constant observed for pCBA could indicate that 275 nm light irradiation does not readily induce formation of reactive oxygen species such as $OH^{\bullet}$ and its degradation solely driven by photolysis. pCBA contains a conjugated benzene ring, carbonyl group on C1 and lone pair electrons on the Cl atom which contributes to its UV absorbance (Figure SI-1). The electronegativity of the Cl atom on C4 creates an electron withdrawing effect on the benzene ring. This can reduce photodegradation efficiency as has been described for other chlorophenols undergoing UV irradiation[40] which explains its minimal photodegradation observed here and by others[37].

Caffeine was similarly degraded to pCBA exhibiting a maximum of 17 % (k_{obs} = 6.61 x 10^{-5} cm^{-2} mJ^{-1}) mean removal at the highest fluence condition and 95% confidence intervals indicate no statistically significant difference in degradation kinetics between pCBA and caffeine (Table 1).

Though caffeine exhibits very high molar absorbance within the relevant emittance range (ε_{275nm} = 9884 M^{-1} cm^{-1}), minimal degradation of caffeine under UV irradiation has been similarly observed in previous work[41–45]. Caffeine absorbs readily within the UV treatment (i.e. 200-300 nm) range due to its extensive electron delocalization across the purine ring system from lone pair electrons on the N atoms, double bonds in the imidazole ring, and carbonyl groups on C2 and C6[43] (Figure SI-1) but lacks significant conjugation across the molecule which contributes to its photostability.

3.1.2 Quantum Yield Determinations

UV LEDs have historically been treated as monochromatic light sources, but by nature, UV LEDs emit polychromatically over wavelength bands (i.e., Figure 2) which are much broader than emittance range of traditional monochromatic (i.e., LP UV) light sources[8]. As such, we calculated and compared both the polychromatic and monochromatic quantum yields (Φ) of each of the above test compounds as previously described (Equation 2 & Equation 3; see Methods)[46]. Calculated quantum yields can be found in Table 2 below. Quantum yields for urea were not calculated due to negligible degradation and poor fit for first-order kinetics (described above; Table 1)

Table 2. Polychromatic ($\Phi_{258-315nm}$) and monochromatic (Φ_{275nm}) quantum yields for target compounds. Brackets indicate 95% confidence intervals.

Analyte	$\Phi_{poly,275nm}$ (mol Es^{-1})	$\Phi_{mono,275nm}$ (mol Es^{-1})	Percent Difference (%)
pCBA	0.0278 [0.0236, 0.0320]	0.0231 [0.0196, 0.0266]	18.5
Caffeine	0.00151 [0.00132, 0.00170]	0.00131 [0.00115, 0.00148]	14.2
Tryptophan	0.050 [0.0485, 0.0510]	0.0478 [0.0465, 0.0490]	4.50
E1	0.864 [0.805, 0.923]	0.879 [0.820, 0.939]	0.893

3.1.2.1 *Comparison of Monochromatic and Polychromatic Quantum Yields*

The calculated 95 % confidence intervals indicate that differences in monochromatic ($\Phi_{\mathrm{mono},275nm}$) and polychromatic ($\Phi_{poly,275nm}$) quantum yields were not statistically significant within analytes (Table 2) but differences in mean values were > 10 % for UV-resistant compounds. For example, $\Phi_{poly,275nm}$ for pCBA and caffeine were mean 18.5 and 14.2 % higher than $\Phi_{\mathrm{mono},275nm}$, respectively, indicating that in these cases, monochromatic quantum yield calculations may underestimate true quantum yield. In contrast, differences in monochromatic and polychromatic values were less pronounced for UV-sensitive analytes. $\Phi_{poly,275nm}$ was < 5 % higher and < 1 % lower than $\Phi_{mono,275nm}$ for tryptophan and E1 respectively, indicating minimal differences in monochromatic and polychromatic quantum yields for these compounds. Li et al. (2022) found that monochromatic quantum yield calculations underestimated true quantum yield values of chlorine species (HOCl & OCl^-) by 5.66 – 14.63 % under 265 & 280 nm UV LED irradiation[47]. In contrast, Pousty et al. (2022) determined that differences between polychromatic and monochromatic quantum yields for uridine were negligible under 279 nm UV LED irradiation and that the studied 279 nm UV LED could be treated as a quasi-monochromatic light source[48]. Accordingly, there may be situations where UV LEDs can be treated as monochromatic light sources without significant error, but this is almost certainly dependant on the emittance wavelength and FWHM of the UV LED light source, as well as the chemical structure, molar absorbance, and subsequent UV-sensitivity of the compound of interest. In most cases, it may be most appropriate to treat these light sources as polychromatic unless the use case has been proven otherwise for a particular light source and compound combination. In the section below, $\Phi_{poly,275nm}$ for all analytes was chosen to provide comparison to the literature.

3.1.2.2 *Discussion of Quantum Yields for pCBA and Caffeine*

Polychromatic and monochromatic quantum yields at 275nm ($\Phi_{poly,275nm}$ & $\Phi_{mono,275nm}$) have not previously been reported in the literature for the target compounds evaluated in this paper.

Calculated mean $\Phi_{poly,275nm}$ for pCBA was 0.0278 mol Es^{-1} in this work (Table 2). Rosenfeldt & Linden (2007) calculated monochromatic (LP UV; 254 nm) and polychromatic (MP UV; 200 – 300 nm) quantum yields of pCBA as 0.013 ± 0.002 mol Es^{-1} and 0.018 ± 0.004 mol Es^{-1}, respectively[37] which are mean 72.5 and 42.8 % lower than is reported in this work. Similarly, Shu et al. (2013) reported $\Phi_{Caffeine}$ under MP UV irradiation as 0.0003 ± 0.001 mol Es^{-1} [49] which is nearly an order of magnitude lower than the calculated $\Phi_{poly,275nm}$ for caffeine in this study (0.00151 mol Es^{-1}).

Differences in reported values could indicate wavelength dependence within these wavelength ranges. Though this is unlikely for pCBA as molar absorbance of is substantially higher at 254 nm in comparison to 275 nm (ε = 3196 vs. 600 M^{-1} cm^{-1} for 254 nm and 275 nm, respectively), this could contribute to discrepancies in quantum yield values for caffeine. Caffeine has an absorbance peak at 274 nm (ε = 9845 M^{-1} cm^{-1}; current work) and another around 207 nm (ε ≈ 25 000; Shu et al. (2013)[49]). The emittance of the 275 nm reactor demonstrates 100 % overlap with the 274 nm emittance band of caffeine, while MP UV light is intermittently distributed across the UVA, UVB, + UV C ranges (i.e., Figure 3). It may be that the peak 275 nm emittance band for the UV LED is able to more effectively facilitate photochemical reactions by targeting the 274 nm absorbance band of caffeine directly than is the spectral emittance of a MP UV lamp which would be distributed across the UV spectrum (as is discussed further for E1 and 17β-E2 in Section 3 below).

Differences in light intensity could also explain variation between calculated values in the literature. Linden & Darby (1997) showed that increasing light intensity in LPUV systems can result in higher apparent quantum yields of uridine[50], but only to a maximum value of 0.4 mW cm^{-2}, after which no further increase was observed up to a maximum of 3.2 mW cm^{-2}. More recently, Rajesh et al. (2025) observed an over two-fold increase in quantum yield of dibromoacetonitile under high power output vs. low power output 265 nm UV LEDs[24]. In this work, the calculated fluence rate of the reactor under uridine actinometry was 249 mW cm^{-2}. There are no commercially available mercury-based systems and no other UV LED systems outside of the reactor type

415 employed in this study, which can produce such high intensity UV light. A conventional system
416 could theoretically be designed to deliver high intensity light but would inevitably also deliver so
417 much heat to a sample that it would be very challenging to mitigate the impact of heat on samples.

418 The kinetic and photochemical behaviour of analytes under this high-intensity UV light source are
419 most likely not directly comparable to lower intensity light sources. This concept warrants further
420 investigation to determine the impacts of drastically different intensities on degradation kinetics.
421 Further, the reactor used in this experiment is flow-through design and has not previously been
422 described for degradation of organic compounds using UV LEDs. The dynamics of each
423 experimental setup likely require individual considerations for the specific water chemistry that is
424 being investigated in an experiment.

425 *3.1.2.3 Discussion of Quantum Yields for Tryptophan and E1*

426 $\Phi_{\text{Tryptophan}}$ varies from below 0.01 to 0.35 based on currently published studies; Callus & Liu (2003)
427 discuss this may be related to differences in electron transfer caused by environmental variations
428 during measurement[51]. Calculated $\Phi_{poly,275nm}$ for tryptophan in this study is within this range of
429 values (0.050 mol Es^{-1}; Table 2) but it is relevant to note that the above reported values are based
430 on fluorescent quantum yield determinations over a variety of wavelength ranges vs. the time-
431 based kinetic quantum yield calculation method employed in this work[46]. Reported quantum yield
432 values for E1 in the literature are also variable and have been reported from 0.065 mol Es^{-1} (10 µg
433 L^{-1}, LP UV irradiation[52]) to 0.35 ± 0.14 mol Es^{-1} (5 ug L^{-1}, LP UV irradiation[43]) and as high as
434 5.14 mol Es^{-1} (1 mg L^{-1}, LP UV irradiation[53]). It is unclear the cause of such large discrepancies
435 in the literature as all three example references above used the same method to calculate quantum
436 yield at the same irradiation wavelength, though Pereira et al. (2012) evaluated concentrations two
437 orders of magnitude or greater than the others described above. The calculated quantum yield for
438 E1 in this study is within the range demonstrated in the literature ($\Phi_{poly,275nm}$ = 0.864 mol Es^{-1})
439 but further work is needed to explain if variation from values previously reported is due to

wavelength dependence (which is discussed further above and in Section 3), differences in calculation, variation in light intensity (as described above), or other factors.

3.1.3 Summary of Findings

This work presents the first demonstration of k_{obs} at 275 nm, $\Phi_{poly,275nm}$ and $\Phi_{mono,275nm}$ for the described compounds and demonstrates the potential of tailored photolysis processes for degradation of TrOCs. This work also provides the first use and application of a novel, flow-through UV LED reactor which allows for substantially higher sample throughput and lower fluence delivery time as compared to traditional collimated beam setups (SI-Text 5, Figure SI-6). This work identified that 275nm UV LED light was highly effective in the removal of E1 & tryptophan by photolysis. Not all target compounds exhibited a similar susceptibility to degradation at UV LED at 275nm. The combination of UV absorbance profile and chemical structure of the target were the two primary governing factors when determining efficacy of photolytic treatment and compounds with higher quantum yields were more susceptible to photolytic degradation. Consideration of each of these features is key in developing bespoke UV LEDs for robust and mercury-free water treatment approaches.

3.2 Part 2: Comparison of UV C LED and Medium-Pressure Mercury Vapour Photolysis for Degradation of Steroid Hormones

In secondary experiments, E1 and another steroid estrogen, 17β-estradiol (17β-E2) were chosen to assess the effectiveness of 275 nm LED irradiation and MP UV irradiation. E1 was chosen due to its demonstration of photodegradability in Part 1 experiments. 17β-E2 was chosen based on its similar structure and absorbance profile to E1 but comparative resistance to photodegradation in comparison to its sister compound[35,54]. Further, both are environmentally relevant TrOCs which cause endocrine disrupting effects in aquatic organisms[55] and evaluation of effective treatment techniques relevant to both municipal and agricultural sectors which are the primary producers of estrogenic waste released into aquatic environments[55–57]. Secondary experiments were conducted

using traditional collimated beam setups described in the Methods. It is relevant to note that the semiconductor chips in the collimated beam reactor evaluated here are paired with those used in the flow-through reactor described in Section 2 experiments, meaning that the emittance spectrum is identical for both systems.

E1 & 17β-E2 were degraded by both light sources but the MP UV system required substantially higher fluence delivery to achieve comparable removal to the 275 nm UV LED system. The MP UV light source also was unable to degrade 17β-E2 below detectable limits even at a fluence of 10 000 mJ cm^{-2} while complete (below detectable limits) removal was achieved at a fluence of 2000 mJ cm^{-2} using the 275nm UV LED light source. These data and the absorbance/emittance spectra of the reactors and analytes are highlighted in Figure 3. Further, the MP UV system only demonstrates 17% overlap in total light emission with the molar absorbance spectra of each estrogen, whereas 275 nm UV LED emittance spectrum demonstrates 100 % overlap with the lower absorbance band of each estrogen. This suggests that, while E1 is likely amenable to photodegradation under MPUV light due to its relative photosensitivity throughout the UV spectrum, MP UV degradation for 17β-E2 may be primarily driven by the generation of radical species from light emitted in the far-UVC region which warrants further investigation. These results show the importance of understanding the character of TrOCs, and tailoring of UV C light sources, when considering UV LEDs vs MP UV treatment systems.

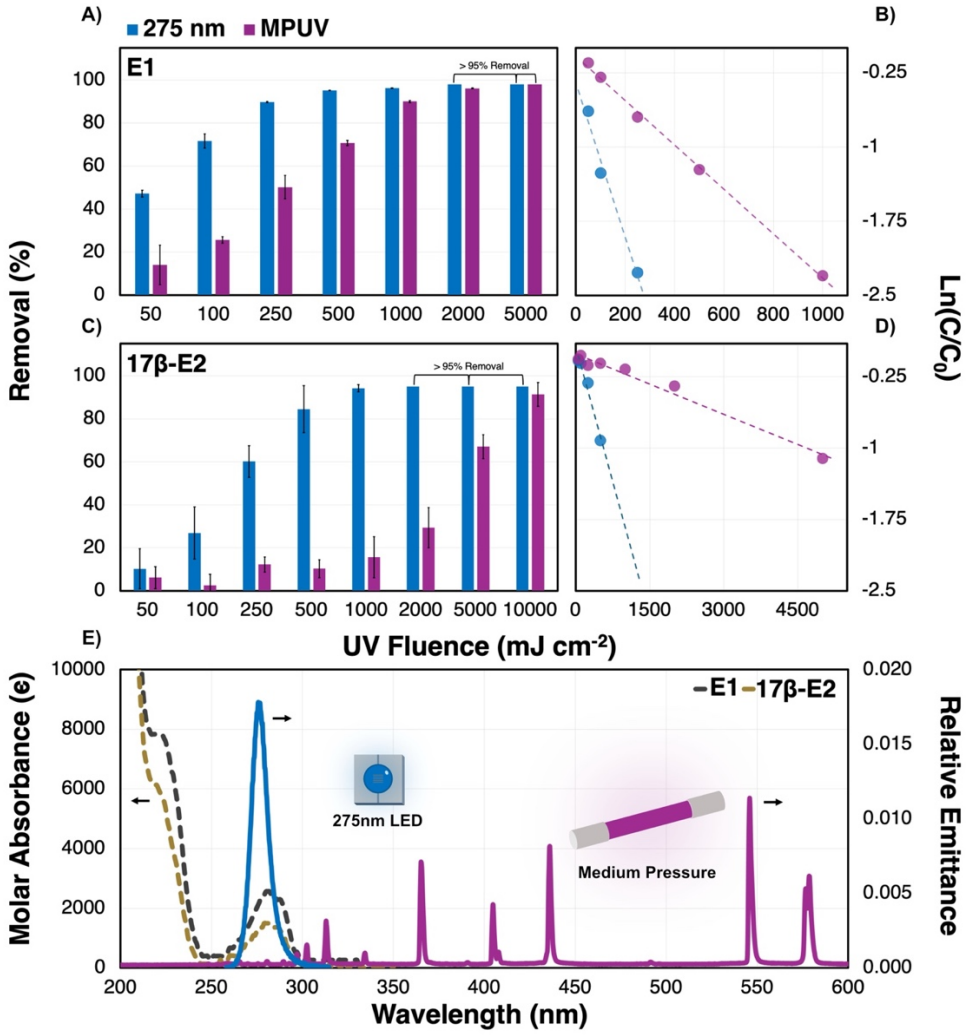

483

484 **Figure 3**. Degradation (A, C) and first-order kinetics (B, D) plots of E1 & 17β-E2 under 275 nm
485 UV LED irradiation from bench-scale 275 nm LED or MP UV collimated beam reactors. Error
486 bars represent one standard deviation from the mean value. Note differences in x-axis values
487 between compounds. Experimental parameters: pH = 7, 2 mM PO_4^{2-} buffer; $[E1]_0$ = 10 μg L^{-1};
488 $[17\beta\text{-}E2]_0$ = 10 μg L^{-1}. n = 3.

3.2.1 *UV C LED and MP UV Degradation of E1*

$\Phi_{poly,275nm}$ and k_{obs} for E1 were similar between 275 nm flow-through reactor (Part 1) and collimated beam (Part 2) experiments, though 95 % confidence intervals indicate statistically significant differences between values (Table 1, Table 3). The mean 15.8 % and 18 % difference observed between first-order rate constants and quantum yields (respectively) is most likely due to differences in reactor intensity (249 mW cm^{-2} (flow-through reactor) vs. 3.62 mW cm^{-2} (collimated beam)). We discussed the implications of this earlier in Section 2 as it pertains to quantum yield and the same discussion would apply here. Similar phenomenon has also been observed for degradation kinetics of other TrOCs; Rajesh et al. (2025) found that increasing the incident irradiance of 265 nm UV LEDs resulted in a 2.3-fold increase in the kinetics rate constant of dibromoacetonitrile even when controlling for fluence[24].

Table 3. Polychromatic ($\Phi_{poly,275nm}$ for the 275nm LED or $\Phi_{poly,MPUV}$ for MP UV lamp) and monochromatic ($\Phi_{mono,275nm}$) quantum yields for target compounds

Analyte	Irradiation Source	Fluence-based rate constant k_{obs} (/x 10^{-3}; cm^2 mJ^{-1})	r^2	Φ_{poly} (mol Es^{-1})	$\Phi_{mono,275nm}$ (mol Es^{-1})	% Difference
E1	275 nm LED	7.87 [7.63, 8.10]	0.9827	0.721 [0.703, 0.740]	0.735 [0.715, 0.756]	1.92
E1	MP UV	2.37 [2.15, 2.61]	0.9949	0.189 [0.177, 0.199]	-	
17β-E2	275 nm LED	4.04 [3.01, 5.06]	0.9712	0.125 [0.0930, 0.156]	0.125 [0.0930, 0.156]	0
17β-E2	MP UV	0.215 [0.183, 0.247]	0.9500	0.0244 [0.0209, 0.0280]	-	

E1 was degraded by > 90% under 275 nm irradiation at 50 % of the fluence required under MP

UV (Figure 3). Fluence-based rate constants were > 3x higher (Table 3) and polychromatic quantum yields were nearly ~ 4x higher under 275 nm irradiation as compared to MP UV (0.721 mol Es^{-1} ($\Phi_{poly,275nm}$) vs 0.189 mol Es^{-1} ($\Phi_{poly,MPUV}$)) indicating wavelength dependence within the 200 – 310 nm region. As described in Section 2, E1 is known to undergo rapid photodecomposition when exposed to light over wide ranges of the UV spectrum[27,31–35] and so effective degradation under both 275 nm and MP UV conditions would be expected. The more effective degradation observed under 275 nm light is almost certainly due targeted nature of the 275 nm reactor emittance over the 281 nm absorbance band of E1 (Figure 3). The peak emittance of the reactor and 281 nm absorbance band of the analyte are overlapping (peak reactor emittance = 275 nm; peak E1 absorbance = 280 – 282 nm, ε = 2569 M^{-1} cm^{-1}) in comparison to the MP UV lamp, which emits sporadically in the 200 – 300 nm primary absorbance range of E1 (Figure 3). E1 also has an absorbance shoulder at ~ 220 nm (ε = 7841 M^{-1} cm^{-1}) and a second absorbance peak at 203 nm (ε = 30 146 M^{-1} cm^{-1}), which could be theoretically targeted by the MP UV lamp. The absorbance peak observed at 281 nm corresponds to E1's lowest energy absorption band[29]. If a photon is absorbed by a compound has energy sufficient to promote a compound to its first excited state and result in a photochemical reaction, the absorption of photons of higher energy will not increase the rate of a photochemical reaction and the additional energy will be lost as heat[46]. Therefore, the light emission by the 275 nm reactor is more efficiently delivering photochemical reactions for E1 removal than the MP UV lamp.

The same photoproduct of estrone as discussed in earlier experiments (consistent with lumiestrone) was detected under both 275 nm and MP UV irradiation. Photoproduct dynamics under 275 nm irradiation were similar to flow-through reactor experiments: peak photoproduct evolution was observed at 250 mJ cm^{-2} as compared to 231 mJ cm^{-2} the 275 nm flow through reactor. The photoproduct was non-detectable at a fluence of 5000 mJ cm^{-2} (Figure 4, Figure SI-5 B). In contrast, peak photoproduct evolution was not observed until 2000 mJ cm^{-2} under MP UV and the photoproduct was still observed at ~51 % of maximum peak response at highest fluence conditions

529 (5000 mJ cm^{-2}; Figure 4, Figure SI-5 C). Accordingly, this tailored wavelength approach to
530 photolytic degradation demonstrates more rapid degradation of E1 and improved reduction in its
531 associated photoproduct as compared to MP UV irradiation.

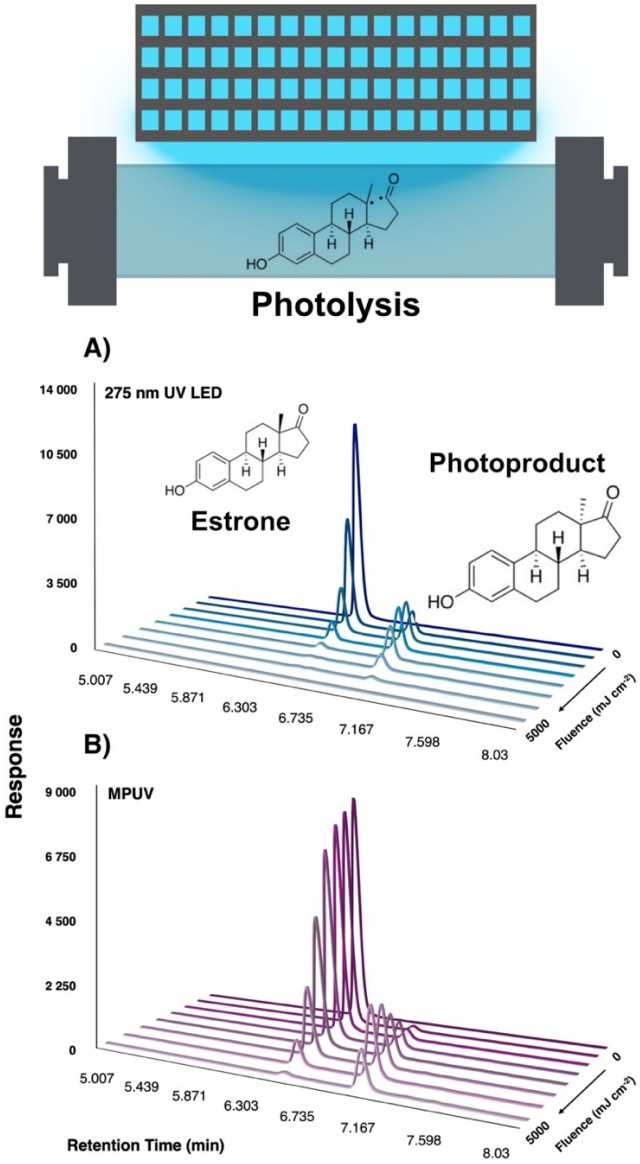

532

533 **Figure 4**. E1 and associated photoproduct response as a function of fluence under 275 nm (A)
534 and MP UV (B) irradiation

3.2.2 *UV C LED and Medium-Pressure Mercury Vapour Degradation of 17β-E2*

17β-E2 was degraded by > 80% under 275 nm irradiation at 5% of the fluence required (500 mJ cm^{-2}) under MP UV (10 000 mJ cm^{-2}), and > 90% under 275 nm irradiation at 10% of the fluence required as compared to under MP UV (Figure 3). Complete (below detectable limits) degradation was observed under 275 nm irradiation at a fluence of 2000 mJ cm^{-2}. In contrast, 17β-E2 was still detectable even at very high (i.e., 10 000 mJ cm^{-2}) fluence conditions under MP UV irradiation. Fluence-based rate constants were also more than an order of magnitude higher under 275 nm irradiation (4.04 x 10^{-3} cm^2 mJ^{-1} vs. 2.15 x 10^{-4} cm^2 mJ^{-1} under 275 nm irradiation and MP UV respectively) and the polychromatic quantum yield was ~ 5x higher under 275 nm irradiation (0.125 mol Es^{-1} ($\Phi_{poly,275nm}$) vs 0.0244 mol Es^{-1} ($\Phi_{poly,MPUV}$)) indicating wavelength dependence within the 200 – 310 nm region (Table 3).

17β-E2 has a very similar structure and absorbance profile to E1 with an absorbance band at 281 nm (ε = 1498 M^{-1} cm^{-1}), an absorbance shoulder at ~ 220 nm (ε = 6129 M^{-1} cm^{-1}) and second absorbance band ~ 200 nm (ε = 31 598 M^{-1} cm^{-2}; Figure 3). It is likely that the same spectral dynamics described above for E1 are also applicable to 17β-E2, i.e., targeted photochemical activation of the lower energy band (~280 nm) by the 275 nm UV C LED can more effectively evoke photochemical reactions than is the polychromatic distribution of light by the MP UV light source. In this case, the reduction in required fluence over commercially available systems is significant (to be redundant, 10 % of the required fluence to achieve 90 % degradation) which has meaningful implications for stakeholders looking for mercury-free UV treatment options to remediate estrogenic compounds (i.e., agriculture, pharmaceutical, municipal, among others[55]).

3.2.3 *Efficiency and Electrical Efficiency Order (EEO) Calculations*

The electrical energy required to achieve 90 % degradation (Electrical Efficiency Order; EEO) of E1 & 17β-E2 under both 275 nm and MP UV irradiation was calculated to determine direct energy

559 cost differences between the two systems (Equation 6, see Methods). Both analytes were degraded
560 at a significantly higher rate under 275 nm irradiation (Table 3) than the MP UV system. The waste
561 heat energy is directed in the same direction as light energy for MP UV systems imparting practical
562 upper boundary conditions for the MP UV system that would not exist for the UV LED system (in
563 which heat and light energy move in opposing directions). High ($\geq$ 2000 mJ cm^{-2}) fluence
564 conditions would be impractical or impossible in a full-scale MP UV system. Nonetheless, for
565 illustrative purpose, EEO values were 25 % higher under 275 nm irradiation for E1 (mean 1.31
566 and 1.02 kwh m^{-3} $order^{-1}$ for the 275 nm UV C LED and MP UV lamp respectively; Table 4) while
567 energy usage was reduced by over four-fold for 17β-E2 under 275 nm conditions with the current
568 3.5 % WPE UV C LED system (2.66 vs 11.34 kwh m^{-3} $order^{-1}$ for the 275 nm UV LED and MP
569 UV lamp respectively). This represents significant potential for direct UV LED photolysis system
570 that is neither practically possible for mercury UV systems and theoretically more efficient for
571 17β-E2 with current LED technology.

572 **Table 4**. EEO values for 17β-E2 & E1 under 275 nm UV LED and MP UV irradiation. Brackets
573 indicate 95 % confidence intervals.

Analyte	Irradiation Source	EEO (kwh m^{-3} $order^{-1}$)
E1	275 nm LED (3.5% WPE)	1.31 [1.27, 1.35]
	MP UV (15% WPE)	1.02 [0.916, 1.13]
17β-E2	275 nm LED (3.5% WPE)	2.66 [1.89, 3.43]
	MP UV (15% WPE)	11.34 [9.78, 12.91]

574 ## 4 Prospects for UV C LEDs as a Climate Robust Treatment Technology

575 UV C LEDs have confirmed effectiveness for full-scale disinfection in drinking water and
576 wastewater[13,58] and have demonstrated ability to replace mercury lamps in most water treatment

applications. Limitations on their wide-spread use have largely been related to historical constraints in power output and energy efficiency. Power outputs of UV C LEDs have improved by over two orders of magnitude (139x) in the last ten years[8], and current efficiency limitations, particularly for UV C LEDs, are not due to the fundamental quantum mechanics of the system but technological limitations[6]. It is projected that technological advances could see the development of more WP efficient UV C LEDs within the next ten years[6] which would only increase practical capability to disrupt water treatment design possibilities.

This work demonstrates the significant use potential of UV C LEDs for removing steroid estrogens from water. Estrogenic compounds are used as feed additives or implants in aquaculture[35,59–61] and agriculture systems[55,62] (respectively), as active ingredients in oral contraceptives and hormone replacement therapies[55,63], and are also present naturally in the human body. These scenarios result in significant inputs of estrogens into municipal treatment plants and the global environment. Steroid estrogens are often not effectively removed or degraded by standard treatment practices employed at municipal wastewater treatment plants[64–68] and these compounds require the addition of chemical agents (to facilitate AOPs), high-pressure membranes (e.g., reverse osmosis (RO) or nanofiltration (NF)), adsorbent materials (e.g., granular activated carbon (GAC)) or ion exchange technologies) to effectively remediate[69]. In the latter cases, processes result in secondary waste streams (e.g., membrane concentrate, exhausted adsorbent, spent ion-exchange resin) which need to be further treated, regenerated, or disposed of, resulting in significant cost, materials waste, and carbon footprint. The current work illustrates the substantial promise of UV LEDs to provide effective, chemical-free, bespoke treatment of steroid estrogens with no secondary waste streams and tailoring in wavelength emittance could see similar applications for a wide range of concerning contaminants.

Future potential could see bespoke UV LED technology design for even recalcitrant compounds such as per- and polyfluoroalkyl substances (PFAS) which require large energy inputs to break C-F bonds (96.8 – 131.6 kcal mol^{-1} [70]). This is no longer an impossibility with current technology

603 trajectory. It is possible for LEDs to approach 100 % WPE under ideal scenarios[71] and current
604 limitations are technological and not fundamental[6]. By the early 21st century, SSLE devices had
605 largely replaced technological illumination alternatives in consumer products such as vacuum
606 tubes and pressured gases due to their improved efficiency, reliability, longer lifetime, and cost
607 effectiveness in comparison to historical counterparts. It is inevitable that the same will be the case
608 for UV LED replacement of mercury-vapour lamps in water treatment. Ultraviolet diodes are on a
609 similar trajectory as visible light diodes were several decades ago. Cathode ray tubes (CRTs) were
610 the primary display technology throughout the mid 20th and early 21st century. The onset of LED-
611 based displays ushered the emergence of 1080p as a standard resolution for televisions and
612 monitors in the early 2010's which resulted in the displacement of CRT televisions. 4k display are
613 now repeating this cycle with 1080p screens. UV LEDs are now at the tipping point of displacing
614 an established technology for disinfection with the use of full-scale UV LED disinfection. This
615 work makes it possible to imagine how advancement in UV LED technology will foster
616 algorithmic-driven water treatment, dual-purpose disinfection/photolysis reactors, and dynamic
617 adjustment of emitted wavelength(s) in large-scale reactors.

618 **5 Conclusions**

619 UV LEDs are a proven breakthrough technology that have significant potential beyond traditional
620 applications such as UV disinfection. This work marks the first characterization, use and
621 implementation of a novel, bench-scale tailored photolytic UV LED reactor. The specific unit that
622 was used in this work contained all 275nm peak emittance UV C LEDs but could be customized
623 to suit any of the currently available UV LED outputs making them broadly applicable to most
624 contaminant degradation applications. Moreover, far-UV C LEDs have more recently become
625 commercially available and expands the design space of tailored treatment approaches for
626 recalcitrant compounds such as PFAS.

627 This characterization study using six different target compounds demonstrated the unique features
628 that tailored light output provides. Estrogenic and amino acid compounds were most susceptible

629 to degradation at 275nm while targets such as caffeine, pCBA, and urea were largely unaffected
630 by exposure to 275nm light. This result suggests that choosing the correct light source to treat
631 target compounds is an important consideration when designing larger photolysis systems using
632 UV LEDs. Evaluation of chemical structure and molar absorbance is necessary to provide an
633 adequate assessment of treatment capabilities and choice of light source, while quantum yield is
634 an excellent proxy for potential treatment outcome and can help to infer potential energy
635 requirements[24].

636 Secondary experiments comparing 275 nm UV C LEDs and a MPUV system further demonstrated
637 the utility of the tailored treatment platform. For 17β-E2, 90% degradation was achieved at
638 fluences 1/10th of that required for similar degradation using the MP UV system. In the case of E1,
639 both the analyte and its associated photoproduct were degraded rapidly under 275 nm irradiation,
640 while E1 degradation rates were significantly lower under MP UV irradiation and the associated
641 photoproduct persisted at even high (5000 mJ cm^{-2}) fluences. Furthermore, the EEO for 17β-E2
642 using the 275 nm UV C LED system was about 4-fold lower that of the MP UV system when using
643 a WPE of 3.5 % (UV C LED) and 15% (MP UV system) respectively. WPE of UV C LEDs is
644 expected to increase substantially in the next ten years[6] which would drastically reduce the energy
645 needs of these systems when compared to conventional mercury lamps in this scenario. This result
646 indicates that tailored use of UV light to treat target compounds can overcome some of the current
647 technological limitations that LEDs have when compared to conventional systems. This benefit is
648 in addition to the many environmental considerations that have been highlighted in this work.

649 Overall, this work shows a novel tool for conducting tailored UV exposure experiments at the
650 bench-scale, determines several previously unreported quantum yields for TrOCs, and provides
651 the groundwork for scaling these technologies via the calculation of energy requirements needed
652 for UV C LEDs when compared to conventional alternatives. The use of tailored UV C LED
653 reactors will lead to a future that does not require the use of chlorine, ozone, or peroxide for the
654 removal of emergent contaminants while also removing mercury from the treatment process. This

discovery and proof of concept has implications across scientific and engineering disciplines given the economic and environmental drivers to eliminate mercury use and reduce the reliance on chemicals in the water treatment process.

6 Acknowledgements

The authors would like to acknowledge funding from the Natural Sciences and Engineering Research Council (NSERC) Alliance "Partnership for Innovation in Climate Change Adaptation in Water & Wastewater Treatment" (grant ALLRP 568507-21), with supporting industry organizations: Halifax Water, LuminUltra Technologies Ltd., Cape Breton Regional Municipality, Mantech Inc., City of Moncton, AquiSense Technologies, AGAT Laboratories, and CBCL Ltd. The authors would also like to acknowledge Dr. Megan Fuller and Carolina Ontiveros for their thoughtful feedback and review of this manuscript, and the assistance of Malavika Parameswaran for her help in completing the bench-scale work carried out during this study.

7 References

(1) European Union. *Regulation - 2024/1849 - EN - EUR-Lex*. https://eur-lex.europa.eu/eli/reg/2024/1849/oj (accessed 2024-11-28).

(2) UNEP. Minamata Convention on Mercury :: Text and Annexes. **2013**.

(3) Ha, E.; Basu, N.; Bose-O'Reilly, S.; Dórea, J. G.; McSorley, E.; Sakamoto, M.; Chan, H. M. Current Progress on Understanding the Impact of Mercury on Human Health. *Environ. Res.* **2017**, *152*, 419–433. https://doi.org/10.1016/j.envres.2016.06.042.

(4) Qiu, G.; Feng, X.; Wang, S.; Shang, L. Environmental Contamination of Mercury from Hg-Mining Areas in Wuchuan, Northeastern Guizhou, China. *Environ. Pollut.* **2006**, *142* (3), 549–558. https://doi.org/10.1016/j.envpol.2005.10.015.

(5) Saldaña-Villanueva, K.; Pérez-Vázquez, F. J.; Ávila-García, I. P.; Méndez-Rodríguez, K. B.; Carrizalez-Yáñez, L.; Gavilán-García, A.; Vargas-Morales, J. M.; Van-Brussel, E.; Diaz-Barriga, F. A Preliminary Study on Health Impacts of Mexican Mercury Mining Workers in a Context of Precarious Employment. *J. Trace Elem. Med. Biol.* **2022**, *71*, 126925. https://doi.org/10.1016/j.jtemb.2022.126925.

(6) Zollner, C. J.; DenBaars, S. P.; Speck, J. S.; Nakamura, S. Germicidal Ultraviolet LEDs: A Review of Applications and Semiconductor Technologies. *Semicond. Sci. Technol.* **2021**, *36* (12), 123001. https://doi.org/10.1088/1361-6641/ac27e7.

(7) Weisbuch, C. Review—On The Search for Efficient Solid State Light Emitters: Past, Present, Future. *ECS J. Solid State Sci. Technol.* **2019**, *9* (1), 016022. https://doi.org/10.1149/2.0392001JSS.

(8) Rauch, K. D.; MacIsaac, S. A.; Reid, B.; Mullin, T. J.; Atkinson, A. J.; Pimentel, A. L.; Stoddart, A. K.; Linden, K. G.; Gagnon, G. A. A Critical Review of Ultra-Violet Light Emitting Diodes as a One Water Disinfection Technology. *Water Res. X* **2024**, *25*, 100271. https://doi.org/10.1016/j.wroa.2024.100271.

(9) Amano, H.; Collazo, R.; Santi, C. D.; Einfeldt, S.; Funato, M.; Glaab, J.; Hagedorn, S.; Hirano, A.; Hirayama, H.; Ishii, R.; Kashima, Y.; Kawakami, Y.; Kirste, R.; Kneissl, M.; Martin, R.; Mehnke, F.; Meneghini, M.; Ougazzaden, A.; Parbrook, P. J.; Rajan, S.; Reddy, P.; Römer, F.; Ruschel, J.; Sarkar, B.; Scholz, F.; Schowalter, L. J.; Shields, P.; Sitar, Z.; Sulmoni, L.; Wang, T.; Wernicke, T.; Weyers, M.; Witzigmann, B.; Wu, Y.-R.; Wunderer, T.; Zhang, Y. The 2020 UV Emitter Roadmap. *J. Phys. Appl. Phys.* **2020**, *53* (50), 503001. https://doi.org/10.1088/1361-6463/aba64c.

(10) Hull, N. M.; Herold, W. H.; Linden, K. G. UV LED Water Disinfection: Validation and Small System Demonstration Study. *AWWA Water Sci.* **2019**, *1* (4). https://doi.org/10.1002/aws2.1148.

(11) Moore, N.; Pousty, D.; Pras, A.; Gehr, R.; Wong, K.; Ma, D.; Linden, K.; Hofmann, R.; Mamane, H.; Beck, S. E. Decentralized Uv Disinfection Systems in Rural Areas or Low-Resource Contexts: A Case Study Compilation. Social Science Research Network: Rochester, NY April 24, 2023. https://doi.org/10.2139/ssrn.4427836.

(12) Gora, S. L.; Rauch, K. D.; Ontiveros, C. C.; Stoddart, A. K.; Gagnon, G. A. Inactivation of Biofilm-Bound Pseudomonas Aeruginosa Bacteria Using UVC Light Emitting Diodes (UVC LEDs). *Water Res.* **2019**, *151*, 193–202. https://doi.org/10.1016/j.watres.2018.12.021.

(13) MacIsaac, S. A.; Reid, B.; Ontiveros, C.; Linden, K. G.; Stoddart, A. K.; Gagnon, G. A. UV LED Wastewater Disinfection: The Future Is upon Us. *Water Res. X* **2024**, *24*, 100236. https://doi.org/10.1016/j.wroa.2024.100236.

(14) Rauch, K. D.; MacIsaac, S. A.; Reid, B.; Mullin, T. J.; Atkinson, A. J.; Pimentel, A. L.; Stoddart, A. K.; Linden, K. G.; Gagnon, G. A. A Critical Review of Ultra-Violet Light Emitting Diodes as a One Water Disinfection Technology. *Water Res. X* **2024**, *25*, 100271. https://doi.org/10.1016/j.wroa.2024.100271.

(15) Rattanakul, S.; Oguma, K. Inactivation Kinetics and Efficiencies of UV-LEDs against Pseudomonas Aeruginosa, Legionella Pneumophila, and Surrogate Microorganisms. *Water Res.* **2018**, *130*, 31–37. https://doi.org/10.1016/j.watres.2017.11.047.

(16) Green, A.; Popović, V.; Pierscianowski, J.; Biancaniello, M.; Warriner, K.; Koutchma, T. Inactivation of Escherichia Coli, Listeria and Salmonella by Single and Multiple Wavelength Ultraviolet-Light Emitting Diodes. *Innov. Food Sci. Emerg. Technol.* **2018**, *47* (November 2017), 353–361. https://doi.org/10.1016/j.ifset.2018.03.019.

(17) Sean A MacIsaac; Kyle D. Rauch; Taylor Prest; Richard M Simons; Graham A. Gagnon; Amina K. Stoddart. Improved Disinfection Performance for 280 Nm LEDs over 254 Nm Low-Pressure UV Lamps in Community Wastewater. **2023**.

(18) Rauch, K. D.; Bennett, J. L.; Stoddart, A. K.; Gagnon, G. A. UV LED Disinfection as a Novel Treatment for Common Salmonid Pathogens. *Sci. Rep.* **2024**, *14* (1), 28392. https://doi.org/10.1038/s41598-024-79347-6.

(19) Rånby, B. Photodegradation and Photo-Oxidation of Synthetic Polymers. *J. Anal. Appl. Pyrolysis* **1989**, *15*, 237–247. https://doi.org/10.1016/0165-2370(89)85037-5.

(20) Ou, H.; Ye, J.; Ma, S.; Wei, C.; Gao, N.; He, J. Degradation of Ciprofloxacin by UV and UV/H2O2 via Multiple-Wavelength Ultraviolet Light-Emitting Diodes: Effectiveness, Intermediates and Antibacterial Activity. *Chem. Eng. J.* **2016**, *289*, 391–401. https://doi.org/10.1016/j.cej.2016.01.006.

(21) Bhat, A. P. Photolysis of Fluorochemicals: Tracking Fluorine, Use of UV-LEDS, and Computational Insights. Ph.D., University of Minnesota, United States -- Minnesota, 2023. https://www.proquest.com/docview/2903728567/abstract/5768B2C6693849B4PQ/1 (accessed 2024-11-18).

(22) Xu, M.-Y.; Zeng, C.; Lin, Y.-L.; Zhang, T.-Y.; Fu, Q.; Zhao, H.-X.; Luo, Z.-N.; Zheng, Z.-X.; Cao, T.-C.; Hu, C.-Y.; Xu, B. Wavelength Dependency and Photosensitizer Effects in UV-LED Photodegradation of Iohexol. *Water Res.* **2024**, *255*, 121477. https://doi.org/10.1016/j.watres.2024.121477.

(23) Eskandarian, M. R.; Choi, H.; Fazli, M.; Rasoulifard, M. H. Effect of UV-LED Wavelengths on Direct Photolytic and TiO2 Photocatalytic Degradation of Emerging Contaminants in Water. *Chem. Eng. J.* **2016**, *300*, 414–422. https://doi.org/10.1016/j.cej.2016.05.049.

(24) Rajesh, L.; Fiorentino, J.; Roberts, T.; McBeath, S. T.; Lanzarini-Lopes, M. Impact of UV-C Irradiance and Wavelength on the Photodegradation of Dibromoacetonitrile. *Environ. Adv.* **2025**, *19*, 100612. https://doi.org/10.1016/j.envadv.2025.100612.

(25) Gérard, V.; Galopin, C.; Ay, E.; Launay, V.; Morlet-Savary, F.; Graff, B.; Lalevée, J. Photostability of L-Tryptophan in Aqueous Solution: Effect of Atmosphere and Antioxidants Addition. *Food Chem.* **2021**, *359*, 129949. https://doi.org/10.1016/j.foodchem.2021.129949.

(26) Igarashi, N.; Onoue, S.; Tsuda, Y. Photoreactivity of Amino Acids: Tryptophan-Induced Photochemical Events via Reactive Oxygen Species Generation. *Anal. Sci.* **2007**, *23* (8), 943–948. https://doi.org/10.2116/analsci.23.943.

(27) Adriano, N.; Ahearn, C.; Black, C.; Cracchiolo, M.; Ghere, D.; Nuñez, A.; Olivan, L.; Patel, R.; Saner, S.; Smith, K. R.; Watkins, B.; Hare, P. M. Solvent- and Wavelength-Dependent Photolysis of Estrone. *Photochem. Photobiol.* **2022**, *98* (4), 783–797. https://doi.org/10.1111/php.13542.

(28) Chan, K. Y.; Courtois, B.; Loose, K.; Hare, P. M. Solvent-Dependent Fluorescence Lifetimes of Estrone, 17β-Estradiol and 17α-Ethinylestradiol. *Photochem. Photobiol.* **2012**, *89* (2), 294–299. https://doi.org/10.1111/php.12011.

(29) Chan, K. Y.; Gavaghan M., B.; Stoeckle, A. W.; Irizarry, K.; Hare, P. M. Solvent Effects on the Steady State Photophysics of Estrone and 17β-Estradiol. *Photochem. Photobiol.* **2011**, *88* (2), 295–303. https://doi.org/10.1111/j.1751-1097.2011.01066.x.

(30) Weinreb, A.; Werner, A. On the Luminescence of Estrogens. *Photochem. Photobiol.* **1974**, *20* (4), 313–321. https://doi.org/10.1111/j.1751-1097.1974.tb06582.x.

(31) Pereira, V. J.; Galinha, J.; Barreto Crespo, M. T.; Matos, C. T.; Crespo, J. G. Integration of Nanofiltration, UV Photolysis, and Advanced Oxidation Processes for the Removal of Hormones from Surface Water Sources. *Sep. Purif. Technol.* **2012**, *95*, 89–96. https://doi.org/10.1016/j.seppur.2012.04.013.

(32) Lin, A. Y.-C.; Reinhard, M. Photodegradation of Common Environmental Pharmaceuticals and Estrogens in River Water. *Environ. Toxicol. Chem.* **2005**, *24* (6), 1303–1309. https://doi.org/10.1897/04-236R.1.

(33) Caupos, E.; Mazellier, P.; Croue, J.-P. Photodegradation of Estrone Enhanced by Dissolved Organic Matter under Simulated Sunlight. *Water Res.* **2011**, *45* (11), 3341–3350. https://doi.org/10.1016/j.watres.2011.03.047.

(34) Ma, X.; Zhang, C.; Deng, J.; Song, Y.; Li, Q.; Guo, Y.; Li, C. Simultaneous Degradation of Estrone, 17β-Estradiol and 17α-Ethinyl Estradiol in an Aqueous UV/H2O2 System. *Int. J. Environ. Res. Public. Health* **2015**, *12* (10), 12016–12029. https://doi.org/10.3390/ijerph121012016.

(35) Bennett, J. L.; Mackie, A. L.; Park, Y.; Gagnon, G. A. Advanced Oxidation Processes for Treatment of 17β-Estradiol and Its Metabolites in Aquaculture Wastewater. *Aquac. Eng.* **2018**, *83*, 40–46. https://doi.org/10.1016/j.aquaeng.2018.08.003.

(36) Trudeau, V. L.; Heyne, B.; Blais, J. M.; Temussi, F.; Atkinson, S. K.; Pakdel, F.; Popesku, J. T.; Marlatt, V. L.; Scaniano, J. C.; Previtera, L.; Lean, D. R. Lumiestrone Is Photochemically Derived from Estrone and May Be Released to the Environment without Detection. *Front. Endocrinol.* **2011**, *2*, 83.

(37) Rosenfeldt, E. J.; Linden, K. G. The ROH,UV Concept to Characterize and the Model UV/H2O2 Process in Natural Waters. *Environ. Sci. Technol.* **2007**, *41* (7), 2548–2553. https://doi.org/10.1021/es062353p.

(38) Lei, Y.; Yu, Y.; Lei, X.; Liang, X.; Cheng, S.; Ouyang, G.; Yang, X. Assessing the Use of Probes and Quenchers for Understanding the Reactive Species in Advanced Oxidation Processes | Environmental Science & Technology. *Env. Sci Technol* **2023**, *57* (13), 5433–5444. https://doi.org/10.1021/acs.est.2c09338.

(39) Han, S.-K.; Nam, S.-N.; Kang, J.-W. OH Radical Monitoring Technologies for AOP Advanced Oxidation Process. *Water Sci. Technol.* **2002**, *46* (11–12), 7–12. https://doi.org/10.2166/wst.2002.0709.

(40) Nong, Y.-J.; Wu, Q.-Y.; Wu, Y.-P.; Lee, J.-W.; Lee, M.-Y.; Wang, W.-L. Far-UVC (UV222) Based Photolysis, Photooxidation, and Photoreduction of Chlorophenols Using a KrCl-Excimer Lamp: Degradation, Dechlorination, and Detoxification. *Water Res.* **2025**, *268*, 122560. https://doi.org/10.1016/j.watres.2024.122560.

(41) Baena-Nogueras, R. M.; González-Mazo, E.; Lara-Martín, P. A. Degradation Kinetics of Pharmaceuticals and Personal Care Products in Surface Waters: Photolysis vs Biodegradation. *Sci. Total Environ.* **2017**, *590–591*, 643–654. https://doi.org/10.1016/j.scitotenv.2017.03.015.

(42) Raschitor, A.; Romero, A.; Sanches, S.; Pereira, V. J.; Crespo, J. G.; Llanos, J. Degradation of Neonicotinoids and Caffeine from Surface Water by Photolysis. *Molecules* **2021**, *26* (23), 7277. https://doi.org/10.3390/molecules26237277.

(43) Carlson, J. C.; Stefan, M. I.; Parnis, J. M.; Metcalfe, C. D. Direct UV Photolysis of Selected Pharmaceuticals, Personal Care Products and Endocrine Disruptors in Aqueous Solution. *Water Res.* **2015**, *84*, 350–361. https://doi.org/10.1016/j.watres.2015.04.013.

(44) Liu, H.; Meng, Y.; Li, J.; Wang, X.; Zhang, T. Mechanistic Insights into UV Photolysis of Carbamazepine and Caffeine: Active Species, Reaction Sites, and Toxicity Evolution. *Chemosphere* **2022**, *308*, 136418. https://doi.org/10.1016/j.chemosphere.2022.136418.

(45) Korekar, G.; Kumar, A.; Ugale, C. Occurrence, Fate, Persistence and Remediation of Caffeine: A Review. *Environ. Sci. Pollut. Res.* **2020**, *27* (28), 34715–34733. https://doi.org/10.1007/s11356-019-06998-8.

(46) Bolton, J. R.; Mayor-Smith, I.; Linden, K. G. Rethinking the Concepts of Fluence (UV Dose) and Fluence Rate: The Importance of Photon-Based Units – A Systemic Review. *Photochem. Photobiol.* **2015**, *91* (6), 1252–1262. https://doi.org/10.1111/php.12512.

(47) Li, G.-Q.; Huo, Z.-Y.; Wu, Q.-Y.; Chen, Z.; Wu, Y.-H.; Lu, Y.; Hu, H.-Y. Photolysis of Free Chlorine and Production of Reactive Radicals in the UV/Chlorine System Using Polychromatic Spectrum LEDs as UV Sources. *Chemosphere* **2022**, *286*, 131828. https://doi.org/10.1016/j.chemosphere.2021.131828.

(48) Pousty, D.; Mamane, H.; Cohen-Yaniv, V.; Bolton, J. R. Ultraviolet Actinometry – Determination of the Incident Photon Flux and Quantum Yields for Photochemical Systems Using Low-Pressure and Ultraviolet Light-Emitting Diode Light Sources. *J. Environ. Chem. Eng.* **2022**, *10* (3), 107947. https://doi.org/10.1016/j.jece.2022.107947.

(49) Shu, Z.; Bolton, J. R.; Belosevic, M.; Gamal El Din, M. Photodegradation of Emerging Micropollutants Using the Medium-Pressure UV/H2O2 Advanced Oxidation Process. *Water Res.* **2013**, *47* (8), 2881–2889. https://doi.org/10.1016/j.watres.2013.02.045.

(50) Linden, K. J.; Darby, J. L. Estimating Effective Germicidal Dose from Medium Pressure UV Lamps. *J. Environ. Eng. 123* (11). https://doi.org/10.1061/(ASCE)0733-9372(1997)123:11(11.

(51) Callis, P. R.; Liu, T. Quantitative Prediction of Fluorescence Quantum Yields for Tryptophan in Proteins. *J. Phys. Chem. B* **2004**, *108* (14), 4248–4259. https://doi.org/10.1021/jp0310551.

(52) Huang, F.; Gao, F.; Li, C.; Campos, L. C. Photodegradation of Free Estrogens Driven by UV Light: Effects of Operation Mode and Water Matrix. *Sci. Total Environ.* **2022**, *835*, 155515. https://doi.org/10.1016/j.scitotenv.2022.155515.

(53) Pereira, V. J.; Galinha, J.; Barreto Crespo, M. T.; Matos, C. T.; Crespo, J. G. Integration of Nanofiltration, UV Photolysis, and Advanced Oxidation Processes for the Removal of Hormones from Surface Water Sources. *Sep. Purif. Technol.* **2012**, *95*, 89–96. https://doi.org/10.1016/j.seppur.2012.04.013.

(54) Ma, X.; Zhang, C.; Deng, J.; Song, Y.; Li, Q.; Guo, Y.; Li, C. Simultaneous Degradation of Estrone, 17β-Estradiol and 17α-Ethinyl Estradiol in an Aqueous UV/H2O2 System. *Int. J. Environ. Res. Public. Health* **2015**, *12* (10), 12016–12029. https://doi.org/10.3390/ijerph121012016.

(55) Adeel, M.; Song, X.; Wang, Y.; Francis, D.; Yang, Y. Environmental Impact of Estrogens on Human, Animal and Plant Life: A Critical Review. *Environ. Int.* **2017**, *99*, 107–119. https://doi.org/10.1016/j.envint.2016.12.010.

(56) Combalbert, S.; Hernandez-Raquet, G. Occurrence, Fate, and Biodegradation of Estrogens in Sewage and Manure. *Appl. Microbiol. Biotechnol.* **2010**, *86* (6), 1671–1692. https://doi.org/10.1007/s00253-010-2547-x.

(57) Lange, I. G.; Daxenberger, A.; Schiffer, B.; Witters, H.; Ibarreta, D.; Meyer, H. H. D. Sex Hormones Originating from Different Livestock Production Systems: Fate and Potential Disrupting Activity in the Environment. *Anal. Chim. Acta* **2002**, *473* (1), 27–37. https://doi.org/10.1016/S0003-2670(02)00748-1.

(58) Jarvis; Autin; Goslan; Hassard. Application of Ultraviolet Light-Emitting Diodes (UV-LED) to Full-Scale Drinking-Water Disinfection. *Water* **2019**, *11* (9), 1894. https://doi.org/10.3390/w11091894.

(59) Park, Y.; Alayafi, A.; Bennett, J. L.; Malloy, D.; Smith, P. M.; Ross, N. W.; Gagnon, G. A.; Donaldson, A. A. Modeling the Fate of Dietary 17B-Estradiol and Its Metabolites in an American Eel (Anguilla Rostrata) Recirculating Aquaculture System. *Aquac. Eng.* **2019**, *86*, 101995. https://doi.org/10.1016/j.aquaeng.2019.101995.

(60) Sweeney, C. L.; Bennett, J. L.; Brown, C. A. M.; Ross, N. W.; Gagnon, G. A. Validation of a QuEChERS Method for Extraction of Estrogens from a Complex Water Matrix and Quantitation via High-Performance Liquid Chromatography-Mass Spectrometry. *Chemosphere* **2021**, *263*, 128315. https://doi.org/10.1016/j.chemosphere.2020.128315.

(61) Sweeney, C. L.; Brown, C. A. M.; Bennett, J. L.; Ross, N. W.; Gagnon, G. A. An Extensive Clean-up Method for Extraction of 17β-Estradiol from Eel Aquaculture Waste Solids for Quantitation via High-Performance Liquid Chromatography Tandem-Mass Spectrometry - ScienceDirect. *Aquaculture* **2021**, *542* (15). https://doi.org/10.1016/j.aquaculture.2021.736873.

(62) Smith, Z. K.; Johnson, B. J. Mechanisms of Steroidal Implants to Improve Beef Cattle Growth: A Review. *J. Appl. Anim. Res.* **2020**, *48* (1), 133–141. https://doi.org/10.1080/09712119.2020.1751642.

(63) Cui, C. W.; Ji, S. L.; Ren, H. Y. Determination of Steroid Estrogens in Wastewater Treatment Plant of A Controceptives Producing Factory. *Environ. Monit. Assess.* **2006**, *121* (1), 409–419. https://doi.org/10.1007/s10661-005-9139-8.

(64) Chimchirian, R. F.; Suri, R. P. S.; Fu, H. Free Synthetic and Natural Estrogen Hormones in Influent and Effluent of Three Municipal Wastewater Treatment Plants. *Water Environ. Res.* **2007**, *79* (9), 969–974. https://doi.org/10.2175/106143007X175843.

(65) de Mes, T.; Zeeman, G.; Lettinga, G. Occurrence and Fate of Estrone, 17b-Estradiol and 17a-Ethynylestradiol in STPs for Domestic Wastewater. *Rev Environ Sci Biotechnol* **2005**, 275–311. https://doi.org/10.1007/s11157-004-3216-2.

(66) Desbrow, C.; Routledge, E. J.; Brighty, G. C.; Sumpter, J. P.; Waldock, M. Identification of Estrogenic Chemicals in STW Effluent. 1. Chemical Fractionation and in Vitro Biological Screening. *Environ. Sci. Technol.* **1998**, *32* (11), 1549–1558. https://doi.org/10.1021/es9707973.

(67) Holeton, C.; Chambers, P. A.; Grace, L. Wastewater Release and Its Impacts on Canadian Waters. *Can. J. Fish. Aquat. Sci.* **2011**, *68* (10), 1836–1859. https://doi.org/10.1139/f2011-096.

(68) Cai, H.; Liu, Y.; Zhang, Z.; Wang, X.; Song, X.; Wen, Y. Advances of Steroid Estrogens Pollution in Waters: A Systematic Review. *Water. Air. Soil Pollut.* **2024**, *236* (1), 64. https://doi.org/10.1007/s11270-024-07673-6.

(69) Silva, C. P.; Otero, M.; Esteves, V. Processes for the Elimination of Estrogenic Steroid Hormones from Water: A Review. *Environ. Pollut.* **2012**, *165*, 38–58. https://doi.org/10.1016/j.envpol.2012.02.002.

(70) Lorpaiboon, W.; Ho, J. High-Level Quantum Chemical Prediction of C-F Bond Dissociation Energies of Perfluoroalkyl Substances. *J. Phys. Chem. A* **2023**, *127* (38), 7943–7953. https://doi.org/10.1021/acs.jpca.3c04750.

(71) Kuritzky, L. Y.; Weisbuch, C.; Speck, J. S. Prospects for 100% Wall-Plug Efficient III-Nitride LEDs. *Opt. Express* **2018**, *26* (13), 16600–16608. https://doi.org/10.1364/OE.26.016600.

(72) Payne, E. M.; Liu, B.; Mullen, L.; Linden, K. G. UV 222 Nm Emission from KrCl* Excimer Lamps Greatly Improves Advanced Oxidation Performance in Water Treatment. *Environ. Sci. Technol. Lett.* **2022**, *9* (9), 779–785. https://doi.org/10.1021/acs.estlett.2c00472.

(73) Zaher, A.; Shehata, N. Recent Advances and Challenges in Management of Urea Wastewater: A Mini Review. *IOP Conf. Ser. Mater. Sci. Eng.* **2021**, *1046* (1), 012021. https://doi.org/10.1088/1757-899X/1046/1/012021.

(74) Jensen, R. A.; Stenmark, S. L. The Ancient Origin of a Second Microbial Pathway for L-Tyrosine Biosynthesis in Prokaryotes. *J. Mol. Evol.* **1975**, *4* (3), 249–259. https://doi.org/10.1007/BF01732984.

(75) Nowicki, S.; Lapworth, D. J.; Ward, J. S. T.; Thomson, P.; Charles, K. Tryptophan-like Fluorescence as a Measure of Microbial Contamination Risk in Groundwater. *Sci. Total Environ.* **2019**, *646*, 782–791. https://doi.org/10.1016/j.scitotenv.2018.07.274.

(76) Wang, C.; Moore, N.; Bircher, K.; Andrews, S.; Hofmann, R. Full-Scale Comparison of UV/H2O2 and UV/Cl2 Advanced Oxidation: The Degradation of Micropollutant Surrogates and the Formation of Disinfection Byproducts. *Water Res.* **2019**, *161*, 448–458. https://doi.org/10.1016/j.watres.2019.06.033.

(77) Cha, Y.; Kim, T.-K.; Lee, J.; Kim, T.; Hong, A.-J.; Zoh, K.-D. Degradation of Iopromide during the UV-LED/Chlorine Reaction: Effect of Wavelength, Radical Contribution, Transformation Products, and Toxicity. *J. Hazard. Mater.* **2022**, *437*, 129371. https://doi.org/10.1016/j.jhazmat.2022.129371.

(78) Zou, X.-Y.; Lin, Y.-L.; Xu, B.; Zhang, T.-Y.; Hu, C.-Y.; Cao, T.-C.; Chu, W.-H.; Pan, Y.; Gao, N.-Y. Enhanced Ronidazole Degradation by UV-LED/Chlorine Compared with Conventional Low-Pressure UV/Chlorine at Neutral and Alkaline pH Values. *Water Res.* **2019**, *160*, 296–303. https://doi.org/10.1016/j.watres.2019.05.072.

(79) Pousty, D.; Mamane, H.; Cohen-Yaniv, V.; Bolton, J. R. Protocol for UVC Uridine Actinometry. *MethodsX* **2023**, *10*, 101957. https://doi.org/10.1016/j.mex.2022.101957.

(80) Rabani, J.; Mamane, H.; Pousty, D.; Bolton, J. R. Practical Chemical Actinometry—A Review. *Photochem. Photobiol.* **2021**, *97* (5), 837–902. https://doi.org/10.1111/php.13429.

(81) Cataldo, F. Uridine as Photochemical Actinometer: Application to LED-UV Flow Reactors. *Eur. Chem. Bull.* **2017**, *6* (9), 405–409.

(82) Bolton, J. R.; Linden, K. G. Standardization of Methods for Fluence (UV Dose) Determination in Bench-Scale UV Experiments. *J. Environ. Eng.* **2003**, *129* (3), 209–215. https://doi.org/10.1061/(ASCE)0733-9372(2003)129:3(209).

(83) MacIsaac, S. A.; Sweeney, C. L.; Gagnon, G. A. Instrument Hacking: Repurposing and Recoding a Multiwell Instrument for Automated, High-Throughput Monochromatic UV Photooxidation of Organic Compounds. *ACS EST Eng.* **2021**, *1* (2), 281–288. https://doi.org/10.1021/acsestengg.0c00123.

(84) US EPA. Definition and Procedure for the Determination of the Method Detection Limit, Revision 2, 2016. https://www.epa.gov/sites/default/files/2016-12/documents/mdl-procedure_rev2_12-13-2016.pdf.